Regularization Techniques for Numerical Approximation of PDEs with Singularities

Anna-Karin Tornberg* Björn Engquist†

Abstract

The rate of convergence for numerical methods approximating differential equations are often drastically reduced from lack of regularity in the solution. Typical examples are problems with singular source terms or discontinuous material coefficients. We shall discuss the technique of local regularization for handling these problems. New numerical methods are presented and analyzed and numerical examples are given. Some serious deficiencies in existing methods are also pointed out.

1 Introduction

Lack of regularity in the solution of a differential equation often reduces the accuracy in numerical simulations. This lack of regularity may, for example, result from singular source terms or discontinuities in the coefficients of the differential operator along interfaces.

A typical error estimate for the numerical approximation,

$$L_h u_h = f_h,$$

of the differential equation,

$$Lu = f,$$

may have the form

$$\|u - u_h\|_{L^2} = Ch^p \|u\|_{H^q}.$$

Here h denotes the maximal step size or element size in the numerical method. The order of the method is p.

If the solution u is not bounded in the H^q-norm the method would in general not reach the p-th order convergence rate. In practice, large or unbounded values of $\|u\|_{H^q}$ often result from local phenomena, as for example, discontinuous coefficients in L or singularities in f or its derivatives.

*Courant Institute of Mathematical Sciences, New York University. Email: tornberg@cims.nyu.edu. Research partially sponsored by PSCI, NADA, KTH and Swedish TFR-grant no 222-2000-434.

†PACM and Department of Mathematics, Princeton University and Department of Mathematics, UCLA. Email: engquist@princeton.edu.

There are mainly two different ways to approach these problems. Either *special numerical methods* are developed for the singularities or the *original problem is regularized* and then approximated numerically. We shall focus on the latter technique in this paper but let us first briefly mention some of the methods in the first class.

A natural technique is *mesh refinement*. In regions where $||u||_{H^q}$ is large, smaller elements are used. If an estimate of type $h^p||u||_{H^q}$ is local a smaller h compensates for a larger norm. When the refinement is done locally, the effect on the overall complexity is limited.

In the finite element method *adjusting the grid* to singular lines or surfaces may improve the overall accuracy. The regularity of u is then higher within each element.

Another possibility is to introduce *special basis functions* in the finite element method, which are adjusted to the analytic solution. Similarly for finite differences *special local differencing* can be introduced, which is satisfied by the solution u to a higher order of accuracy. One successful example is the immersed interface method by LeVeque and Li [9]. Interface and boundary conditions can also be introduced weakly. Innovative weak methods are given by Glowinski [6] and Hesthaven [5] and their collaborators.

Even if the solution to a formally higher order method contains a substantial error component due to the local reduction in regularity of u, it may be possible to *post process* the numerical solution in order to recover the higher order of accuracy in the smooth part of u, see Abarbanel et al. [1].

In the *regularization technique* coefficients and source terms with singularities or singularities in derivatives are replaced by functions of higher regularity. The original functions are only modified in a small zone around the singularities. The regularized problem is then numerically approximated.

An advantage with the regularization technique is that standard numerical methods for regular solutions can be used. It is also possible to apply the method to simple uniform Eulerian grids. This is particularly important for time dependent partial differential equations when also the location of the interfaces changes with time. Dynamic regridding is computationally costly and the necessary interpolation between grids is a source of error.

Regularization for the immersed boundary method was introduced by Peskin [10, 11], and has been used in various applications. It is a natural technique if the location of the interface with singularities is computed by the level set method. The distance to the interface is then given explicitly and can be used in the design of the regularization, see the work by Osher and collaborators, [12].

We present the general framework in section 2 and analyze the regularization of source terms in section 3. Certain moment conditions are required for high accuracy and they are the same as in other related problems [2, 4, 15]. In section 4 we will see that the standard moment conditions are not enough to obtain arbitrarily high order of accuracy. New conditions are needed that are related to homogenization theory [3]. The techniques for interfaces are extended to boundary conditions in section 5 where also two other practical applications are commented on. In the final section we study narrow regularization zones and show that some existing methods may exhibit $O(1)$ errors. We also introduce a new scheme that is derived from its properties in the Fourier domain. Throughout the paper we first consider simple model problems and then discuss generalizations.

2 The Basic Framework

Let us consider a differential equation

$$Lu = f \tag{4}$$

with singularities or singularities in the derivatives either in the source term f or in the coefficients of L. We replace (4) by a regularized equation

$$L_\varepsilon u_\varepsilon = f_\varepsilon \tag{5}$$

where 2ε denote the width of the zone in which the singular functions of (4) have been modified. See figure 1 for typical examples of regularizations which will be used in the later sections. This one dimensional case naturally generalizes to higher dimensions. See section 3.

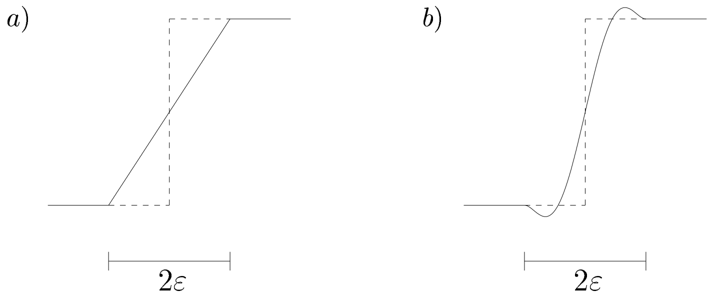

Figure 1: Examples of regularization of the Heaviside function. (a) $H_\varepsilon \in C^0$, (b) $H_\varepsilon \in C^1$. The regularized function in (b) also satisfies higher order moment conditions.

The numerical regularization technique introduces two types of errors: the analytical error between the solutions of the original problem (4) and the regularized problem (5), $(u - u_\varepsilon)$, and the error from the discrete approximation of the regularized problem $(u_\varepsilon - u_{\varepsilon h})$,

$$\|u - u_{\varepsilon h}\| \leq \|u - u_\varepsilon\| + \|u_\varepsilon - u_{\varepsilon h}\| = I + II. \tag{6}$$

We shall here mainly focus on the analytic regularization error and study the numerical error more in detail in a forthcoming paper. Moment conditions will play an important role in the analysis of I. They enter naturally and have been used earlier in similar situations. Examples are the work by Beale and Majda on vortex blob methods [2], by Beylkin on fast Fourier transforms of nonsmooth functions [4] and by Tornberg on quadrature [15].

The regularized functions in the case of singular forces

$$Lu_\varepsilon = f_\varepsilon \tag{7}$$

must satisfy different properties than the functions in the case of singular coefficients,

$$L_\varepsilon u_\varepsilon = f. \tag{8}$$

The standard moment conditions work well for (7) but not always for (8). In the general regularized discontinuous coefficient problem there is an interaction between u_ε and the rapid change of the regularized coefficients near the original singularity that can not be accounted for by the usual moment conditions. The regularizations for (7) and (8) are studied separately in the following sections.

The numerical error (II) depends on the overall order of the numerical method, the number of bounded derivatives of u_ε after regularization and the size of these derivatives in domains where the equations have been modified.

This error will typically have the form

$$II = \mathcal{O}(h^p + h^r + \varepsilon^{-s}h^p) \tag{9}$$

where p is the order accuracy of the numerical method when applied to smooth problems. The h^p-term originates from the numerical error outside of the zone of regularization and the h^r-term is determined by the level of regularity after regularization. Let, for example, the simple equation,

$$\begin{aligned} &\frac{\partial u}{\partial x} = H(x), \qquad -1 < x < 1 \\ &u(-1) = 0 \end{aligned}$$

be regularized by replacing the Heaviside function $H(x)$ with $H_\varepsilon(x)$ from figure 1a. The singularities of $\frac{d^2 H_\varepsilon}{dx^w}$ at $x = -\varepsilon, \varepsilon$ will give $r = 2$ for standard discretizations. This follows from

$$u_\varepsilon(x) = \int_{-1}^{x} H_\varepsilon(\xi) d\xi$$

and the analysis of quadrature errors in [15].

The last term $\varepsilon^{-s}h^p$ represents the error from the potential rapid change of u_ε in the regularization zone. The negative powers of ε is a measure of the relevant derivatives of u_ε and depend on the particular numerical method.

We will see in the following sections that the analytical error I is of the form $O(\varepsilon^{m+2})$, where m is related to some moment conditions for the approximations. If we assume that $\varepsilon^{-s}h^p$ is the largest term in (9) the optimal choice of ε follows from $\varepsilon^{m+2} \sim \varepsilon^{-s}h^p$ or $\varepsilon = O(h^{p/(m+s+2)})$.

The form of (9) depends on the particular numerical method and is based on asymptotic estimates. It is practically desirable not to have ε much larger than h and then the asymptotic form of the estimate (9) is less accurate.

3 Regularization of Source Terms

Consider the ordinary differential equation,

$$\begin{aligned}&\frac{du}{dx} = a(x)u + f(x), \qquad -1 < x < 1, \\ &u(-1) = 0, \\ &a(x) \geq \tilde{a} > 0,\end{aligned} \tag{10}$$

with the solution

$$u(x) = \int_{-1}^{x} e^{\int_{\varepsilon}^{x} a(\eta)d\eta} f(\xi)d\xi + e^{\int_{-1}^{x} a(\eta)d\eta} u(-1). \tag{11}$$

Let $a(x)$ be smooth and $f(x)$ discontinuous at $x = 0$, $a \in C^{\tilde{k}}[-1,1]$.

Equation (10) is now replaced by the regularized problem,

$$\frac{du_\varepsilon}{dx} = a(x)u_\varepsilon + f_\varepsilon(x) \tag{12}$$

Using (11) and subtracting the solutions of (10) and (12) gives,

$$u(x) - u_\varepsilon(x) = \int_{-1}^{x} e^{\int_{\xi}^{x} a(\eta)d\eta}(f(\xi) - f_\varepsilon(\xi))d\xi.$$

We are interested in the solution away from the regularized zone. For $x \leq \varepsilon$, $u \equiv u_\varepsilon$, and for $x \geq \varepsilon$,

$$u(x) - u_\varepsilon(x) = e^{\int_{\varepsilon}^{x} a(\eta)d\eta}(u(\varepsilon) - u_\varepsilon(\varepsilon)) = e^{\int_{\varepsilon}^{x} a(\eta)d\eta} \int_{-\varepsilon}^{\varepsilon} e^{\int_{\xi}^{\varepsilon} a(\eta)d\eta}(f(\xi) - f_\varepsilon(\xi))d\xi.$$

To obtain this formula, we have used (11) and the fact that $f_\varepsilon(x) = f(x)$, $|x| \geq \varepsilon$. After Taylor expansion of $e^{\int_{\xi}^{\varepsilon} a(\eta)d\eta}$ as a function of ξ we get,

$$u(\varepsilon) - u_\varepsilon(\varepsilon) = \int_{-\varepsilon}^{\varepsilon} \left(\sum_{j=0}^{m} \tilde{a}_j \xi^j + O(\xi^{m+1}) \right) (f(\xi) - f_\varepsilon(\xi))d\xi,$$

where $\tilde{a}_j$ denotes the coefficient in the Taylor series. This yields the analytic regularization error estimate

$$|u(x) - u_\varepsilon(x)| \leq C\varepsilon^{m+2}, \ x \geq \varepsilon \tag{13}$$

if the following moment conditions are valid,

$$\int_{-\varepsilon}^{\varepsilon} \xi^j (f(\xi) - f_\varepsilon(\xi))d\xi = 0, \quad j = 0, \ldots, m. \tag{14}$$

The moment conditions (14) control the analytical error. The regularity of u_ε follows from the solutions formula of type (11),

$$\begin{gathered} u_\varepsilon \in C^{\min(k,\tilde{k})+1}[-1,1] \\ \left|\frac{d^\nu u_\varepsilon}{dx^\nu}\right| \leq C\varepsilon^{-\nu},\ \nu \leq \min(k,\tilde{k})+1,\ -1 < x < 1. \end{gathered} \tag{15}$$

where $\tilde{k}$ denotes the regularity of $a(x)$ and k that of $f_\varepsilon(x)$. Formula (15) follows from scaling. The power of ε also depends on the order of the singularity of f at $x = 0$. If, for example, $f = \delta(x)$ then,

$$\left|\frac{d^\nu u_\varepsilon}{dx^\nu}\right| \leq C\varepsilon^{-(\nu+1)}. \tag{16}$$

We can use piecewise polynomials to construct approximations to discontinuous or singular functions of δ-function type. Any number of moment conditions and regularity requirements can be fulfilled by using higher order polynomials, [15].

A discontinuous source term $f(x)$ can be expressed as $f(x) = f_1(x) + H(x)\left(f_2(x) - f_1(x)\right)$, where $H(x)$ is the Heaviside function and $f(x) = f_1(x)$ for $x < 0$ and $f(x) = f_2(x)$ for $x > 0$. The approximate function $f_\varepsilon(x)$, can be written the same way, with $H(x)$ replaced by $H_\varepsilon(x)$.

We define the approximation

$$H_\varepsilon^{m,k}(x) = \begin{cases} 0 & x < -\varepsilon, \\ \nu^{m,k}(x/\varepsilon) & |x| \leq \varepsilon, \\ 1 & x > \varepsilon, \end{cases} \tag{17}$$

where $\nu^{m,k}(\xi)$ is a smooth transition function in $-1 \leq \xi \leq 1$ such that $\nu(-1) = 0$ and $\nu(1) = 1$. The subscript m denotes the number of moment conditions that are fulfilled for this approximation. The index k denotes the regularity, i.e. $H_\varepsilon^{m,k}(x) \in C^k$.

In our numerical experiments, we will use the following functions

$$\begin{aligned} \nu^{0,0}(\xi) &= \frac{1}{2}(1+\xi) \\ \nu^{2,1}(\xi) &= \frac{1}{2} + \frac{1}{32}\left(45\xi - 50\xi^3 + 21\xi^5\right), \\ \nu^{2,2}(\xi) &= \frac{1}{2} + \frac{1}{64}\left(105\xi - 175\xi^3 + 147\xi^5 - 45\xi^7\right) \\ \nu^{4,1}(\xi) &= \frac{1}{2} + \frac{1}{256}\left(525\xi - 1225\xi^3 + 1323\xi^5 - 495\xi^7\right), \end{aligned} \tag{18}$$

to define corresponding Heaviside approximations $H_\varepsilon^{m,k}$. The Heaviside approximations $H_\varepsilon^{0,0}$ and $H_\varepsilon^{2,1}$ are shown in figure 1 in the previous section.

If $f(x) = \delta(x)$, piecewise polynomials can be used in a similar fashion to define approximations $\delta_\varepsilon^{m,k}(x) \in C^k$ that fulfills m moment conditions. See figure 2 for a plot of two different approximations.

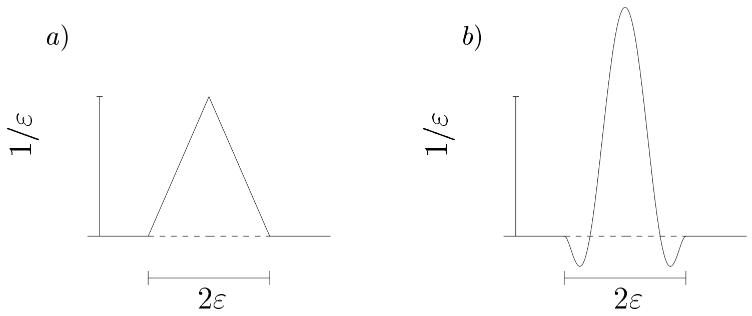

Figure 2: Delta function approximations $\delta_\varepsilon^{0,0}$ and $\delta_\varepsilon^{3,1}$.

Let us define

$$f(x) = \begin{cases} 0.25e^{-x}, & x < x^* \\ e^{-2x}, & x > x^*, \end{cases} \tag{19}$$

and let $a(x) = 0.5$. The solution to (10) is then given by

$$u(x) = \begin{cases} u_1(x) = -\frac{1}{6}(e^{-x} - e^{0.5x+0.5+1}), & -1 \leq x \leq x^* \\ u_2(x) = u_1(x^*)\, e^{0.5(x-x^*)} - \frac{2}{5}(e^{-2x} - e^{0.5x-2.5*x^*}), & x^* < x \leq 1 \end{cases} \tag{20}$$

To avoid cancellation of errors due to grid symmetries, we pick the location of the discontinuity (x^*) to be some irregular number close to 0, instead of exactly zero as was the case in the analysis above.

We use a fourth order Runge-Kutta scheme to march from $x = -1$ to $x = 1$, and we measure the error at $x = 1$ compared to the analytical solution. Typically, for a fixed step size $h = 2/N$, the error will be dominated by numerical errors for small values of ε. As we increase ε, the analytical error will start to dominate, see figure 3. In between, there is a region where the errors are about the same order.

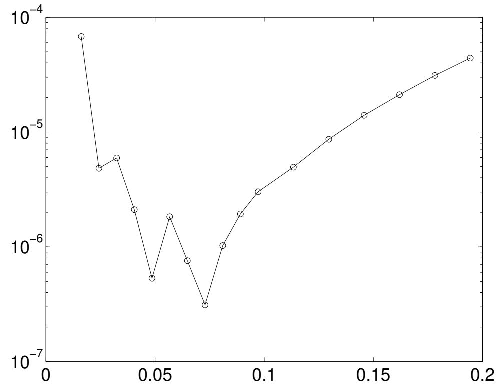

Figure 3: Typical end point error (error at $x = 1$) as a function of ε.

Now, we want to study the analytical error as a function of ε. To make the numerical errors negligible, we therefore use a small step size $h = 2/N$, with N=6400. In figure 4, the endpoint error is plotted for different values of ε. The analytical error is predicted to be proportional to ε^{m+2} for $H_\varepsilon^{m,k}$, and the results agree well with this prediction. In the case of $H_\varepsilon^{4,1}$, the analytical error is proportional to ε^6, and ε must be large before we can see this behaviour, see the right plot in the figure.

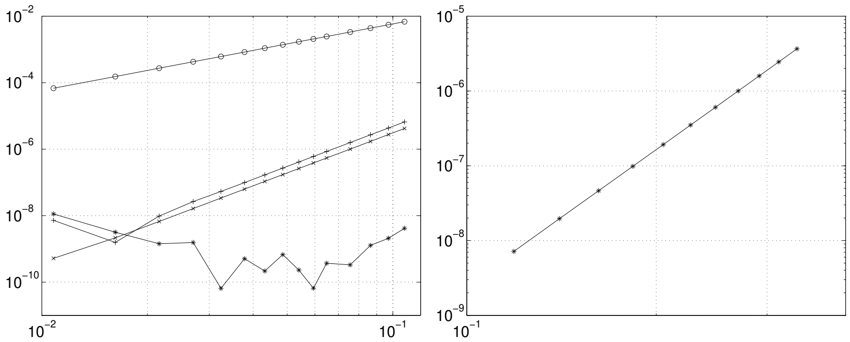

Figure 4: Plot of end point error (error at $x = 1$) versus ε for different approximations of the Heaviside function: $H_\varepsilon^{0,0}$ (-o-), $H_\varepsilon^{2,1}$ (-+-), $H_\varepsilon^{2,2}$ (-x-), $H_\varepsilon^{4,1}$ (-∗-). The slopes correspond to ε^p, where p is approximately 2, 4 and 4 for the first three approximations. The analytical error for $H_\varepsilon^{4,1}$ is still so small, that we need to use even larger values of ε to see the analytical error clearly. In the right figure, the error for $H_\varepsilon^{4,1}$ are shown for larger values of ε. The slope here corresponds to ε^p, where p is approximately 6.

The techniques generalizes to more than one dimension and to wider classes of differential equations.

Assume that the interface $\Gamma \subset \Omega \subset \mathbb{R}^n$ contains the singularities and that Γ separates the domain of the independent variables Ω into two parts Ω_1 and Ω_2. The regularization in the normal direction to Γ is defined using a signed distance function $d(x),\ x \in \Omega$. For the regular Heaviside function (H_ε^n) in $\mathbb{R}^n$, with discontinuity at $x \in \Gamma$ we have,

$$\begin{aligned} H_\varepsilon^n(x) &= H_\varepsilon(d(x)) \\ d(x) &= \begin{cases} \operatorname{dist}(x,\Gamma), & x \in \Omega_1 \\ -\operatorname{dist}(x,\Gamma), & x \in \Omega_2 \end{cases} \end{aligned}$$

The signed distance function is a natural bi-product if the interface tracking was done by the level set method, [12].

The extension to wider classes of differential equations follows from the close relation between solution operators for differential equations and integral operators. The theory from approximation of definite integrals [15] can be applied.

For general elliptic equations with smooth coefficients the solution operator is given by an integral expression

$$Lu = f(x) \qquad x \in \Omega$$
$$u(x) = \int_\Omega K(x,\xi)f(\xi)d\xi.$$

where $K(x,\xi)$ is smooth for $x \neq \xi$. Assume that f is regular outside Γ and that the distance $\mathrm{dist}(x,\Gamma) > \varepsilon$,

$$u(x) - u_\varepsilon(x) = \int_\Omega K(x,\xi)(f(\xi) - f_\varepsilon(\xi))d\xi \tag{21}$$

Let us partition the domain Ω into smaller subdomains

$$\Omega = \cup_{j=1}^J \Omega_j$$

and assuming that Γ is smooth, transform the independent variables $\xi \to \tilde{\xi}^{(j)}$, $\Omega_j \to \tilde{\Omega}_j$ such that Γ corresponds to $\xi_1^{(j)} = 0$ for the new variable $\tilde{\xi}^{(j)} \in \Omega_j$. Formula (21) can then be written

$$u(x) - u_\varepsilon(x) = \sum_{j=1}^J \int_{\tilde{\Omega}_j} \tilde{K}(x,\tilde{\xi}^{(j)})J_j(\tilde{\xi}^j)(\tilde{f}(\tilde{\xi}^{(j)}) - \tilde{f}_\varepsilon(\tilde{\xi}^{(j)}))d\xi^{(j)}.$$

We Taylor expand the smooth function $\tilde{K}J_j$ with respect to $\tilde{\xi}_1^{(j)}$ and integrate with respect to $\tilde{\xi}_1^{(j)}$ and the tangent variables $\tilde{\xi}_T^{(j)}, (\tilde{\xi}^{(j)} = (\tilde{\xi}_1^{(j)}, \tilde{\xi}_T^{(j)}))$,

$$u(x) - u_\xi(x) = \textstyle\sum_{j=1}^J \int \int_{\tilde{\Omega}_j} \left(\sum_{k=1}^m R_{jk}(\tilde{\xi}_T^{(j)})(\tilde{\xi}_1^{(j)})^k + O((\tilde{\xi}_1^{(j)})^{m+1})\right)$$
$$(\tilde{f}(\tilde{\xi}_1^{(j)}, \tilde{\xi}_T^{(j)}) - \tilde{f}_\varepsilon(\tilde{\xi}_1^{(j)}, \tilde{\xi}_T^{(j)}))d\xi_1^{(j)}d\tilde{\xi}_T^{(j)}.$$

The $R_{jk}(\tilde{\xi}_T^{(j)})$ are the coefficient of the Taylor expansion. The estimate based on moment conditions of the analytic regularization error (13) in the simple one dimensional case is thus valid for much wider classes of problems. If the operator L is hyperbolic the technique is still useful but the error estimate not as clean due to the property of propagation of singularities for hyperbolic operators.

The moment conditions can also be expressed in Fourier space. Consider a regularization $\delta_\varepsilon(x),\ x \in \mathbb{R}^1$, of a δ-function source term,

$$\begin{aligned} \delta_\varepsilon(x) &= \frac{1}{\varepsilon}\varphi_F(x/\varepsilon), \\ \varphi_F(\xi) &= \frac{1}{2\pi}\int_{-\infty}^{\infty} \hat{\varphi}_F(\omega)e^{i\omega\xi}d\omega \\ \hat{\varphi}_F(\omega) &= \int_{-\infty}^{\infty} \varphi_F(\xi)e^{-i\omega\xi}d\xi. \end{aligned}$$

If we require $\hat{\varphi}_F(0) = 1$, we have with $\xi = x/\varepsilon$,

$$\int_{-\infty}^{\infty} \delta_\varepsilon(x)dx = \int_{-\infty}^{\infty} \varphi_F(\xi)d\xi = \hat{\varphi}_F(0) = 1,$$

and the condition that the mass is 1 is thus fulfilled. Since

$$\frac{\partial^p}{\partial \omega^p}\hat{\varphi}_F(\omega)|_{\omega=0} = (-i)^p \int_{-\infty}^{\infty} \varphi_F(\xi)\xi^p d\xi,$$

it follows that

$$\frac{\partial^p}{\partial \omega^p}\hat{\varphi}_F(\omega)|_{\omega=0} = 0 \Leftrightarrow \int_{-\infty}^{\infty} \varphi_F(\xi)\xi^p d\xi = 0. \tag{22}$$

It is possible to define functions $\hat{\varphi}_F(\omega) \in C^\infty(\mathbb{R})$ such that (22) is true for all p. Therefore, there exist approximations $\delta_F(t)$, so that all moments are zero. The regularity of $\delta_\varepsilon(x)$ is linked to the decay of $\hat{\varphi}_F(\omega)$ at infinity. If $\hat{\varphi}_F(\omega)$ has compact support $\delta_\varepsilon(x) \in C^\infty(\mathbb{R})$. The constraint that $\hat{\varphi}_F(\omega)$ should have compact support and have all its derivatives zero at $\omega = 0$ however forces the decay as a function of x of the corresponding δ-function approximation not to be rapid enough for practical computations.

4 Regularization of Coefficients

The coefficients in a differential operator typically represent material properties. A domain with different materials thus results in a differential operator with discontinuous coefficients. We shall follow the outline in section 3 and start with a simple one dimensional example.

$$\begin{aligned} &\frac{du(x)}{dx} = a(x)u(x) + f(x), \quad -1 < x < 1. \\ &u(-1) = 0 \end{aligned} \tag{23}$$

Based on the solution formula (11) the error formula will then be,

$$u(x) - u_\varepsilon(x) = \int_{-1}^{x} \left(e^{\int_\xi^x a(\eta)d\eta} - e^{\int_\xi^x a_\varepsilon(\eta)d\eta} \right) f(\xi)d\xi. \tag{24}$$

Here the matching conditions are more complex and illustrates the effect of interaction in the transition zone, $-\varepsilon < x < \varepsilon$. It is, however, quite easy to see that the lowest order condition is the same as for the source term case. From (24) and (11) we have for $x \geq \varepsilon$,

$$u(x) - u_\varepsilon(x) = e^{\int_\varepsilon^x a(\eta)d\eta}(u(\varepsilon) - u_\varepsilon(\varepsilon)),$$

where

$$\begin{aligned} u(\varepsilon) - u_\varepsilon(\varepsilon) = &\int_{-\varepsilon}^{\varepsilon} (e^{\int_\xi^\varepsilon a(\eta)d\eta} - e^{\int_\xi^\varepsilon a_\varepsilon(\eta)d\eta})\, f(\xi)\, d\xi \\ &+ (e^{\int_{-\varepsilon}^\varepsilon a(\eta)d\eta} - e^{\int_{-\varepsilon}^\varepsilon a_\varepsilon(\eta)d\eta})u(-\varepsilon). \end{aligned} \tag{26}$$

With $A(\xi) = \int_\xi^\varepsilon a(\eta)d\eta$ and $A_\varepsilon(\xi) = \int_\xi^\varepsilon a_\varepsilon(\eta)d\eta$ we get

$$\begin{aligned} u(\varepsilon) - u_\varepsilon(\varepsilon) = &\int_{-\varepsilon}^{\varepsilon} (A(\xi) - A_\varepsilon(\xi) + \frac{1}{2}(A(\xi)^2 - A_\varepsilon(\xi)^2))\, f(\xi)\, d\xi \\ &+ \int_{-\varepsilon}^{\varepsilon} O(|A(\xi)|^3 + |A_\varepsilon(\xi)|^3)\, f(\xi)\, d\xi \\ &+ (A(-\varepsilon) - A_\varepsilon(-\varepsilon))u(-\varepsilon). \end{aligned} \tag{27}$$

The condition

$$\int_{-\varepsilon}^{\varepsilon} (a(\xi) - a_\varepsilon(\xi))d\xi = 0, \tag{28}$$

thus implies,

$$|u(x) - u_\varepsilon(x)| \le C\varepsilon^2, \quad -1 < x < 1, \quad |x| \ge \varepsilon, \tag{29}$$

and if also

$$\int_{-\varepsilon}^{\varepsilon} \xi\, (a(\xi) - a_\varepsilon(\xi))\, d\xi = 0 \tag{30}$$

we have

$$|u(x) - u_\varepsilon(x)| \le C\varepsilon^3, \; -1 < x < 1, \; |x| > \varepsilon. \tag{31}$$

The first estimate (29) follows directly from (28), which is equivalent to $A(-\varepsilon) - A_\varepsilon(-\varepsilon) = 0$, and $|A(\xi)| \le C\varepsilon$, $|A_\varepsilon(\xi)| \le C\varepsilon\ \forall \xi$. The higher order estimate (31) is less direct and follows from (30) after integration by parts,

$$\begin{aligned} 0 &= \int_{-\varepsilon}^{\varepsilon} \xi(a(\xi) - a_\varepsilon(\xi))\, d\xi \\ &= \int_{-\varepsilon}^{\varepsilon} \int_{\xi}^{\varepsilon} (a(\eta) - a_\varepsilon(\eta))\, d\eta\, d\xi + \int_{-\varepsilon}^{\varepsilon} (a(\eta) - a_\varepsilon(\eta))\, d\eta \\ &= \int_{-\varepsilon}^{\varepsilon} (A(\xi) - A_\varepsilon(\xi))\, d\xi + A(-\varepsilon) - A_\varepsilon(-\varepsilon) \\ &= \int_{-\varepsilon}^{\varepsilon} (A(\xi) - A_\varepsilon(\xi))\, d\xi \end{aligned} \tag{32}$$

This formula, together with $f(\xi) = f(0) + O(\xi)$ gives the estimate (31).

The third order estimate is the best result we can get, no matter how many moment conditions

$$\int_{-\varepsilon}^{\varepsilon} \xi^j\, (a(\xi) - a_2(\xi))d\xi = 0, \quad j = 0, \ldots, m. \tag{33}$$

we enforce, i.e how large we set m. This is in contrast to the source term case for which arbitrary high order in ε can be achieved by the moment conditions. It is the quadratic terms $(A(\xi)^2 - A_\varepsilon(\xi)^2)$ in (27) that limit the order. This limitation of the order can be seen from counter examples and from the numerical experiments below.

The solution to (23) with

$$a(x) = a_1 + H(x - x^*)(a_2 - a_1), \tag{34}$$

$a_1 = -4$, $a_2 = -2$, and $f(x) = e^x$, is given by

$$u(x) = \begin{cases} u_1(x) = \frac{1}{5}(e^x - e^{-4x-5}), & -1 < x \le x^* \\ u_2(x) = u_1(x^*)\, e^{-2(x-x^*)} + \frac{1}{3}(e^x - e^{-2x-x*}), & x^* < x \le 1 \end{cases} \tag{35}$$

In this numerical example we set the location of the discontinuity to be $x = x^*$ instead of $x = 0$, which was used in the analysis above. To avoid cancellation of errors due to grid symmetries, we pick x^* to be some irregular number close to 0.

We replace the Heaviside function in (34) by the approximations $H_\varepsilon^{m,k}$ introduced in the previous section. We again use a fourth order Runge-Kutta scheme, to march from $x = -1$ to $x = 1$. We measure the error at $x = 1$ compared to the analytical solution. Again, we want to study the analytical error, and we therefore use a small step size $h = 2/N$, with N=6400, to make the numerical errors negligible. In figure 5, the endpoint error is plotted for different values of ε. The analytical error is predicted to be proportional to $\varepsilon^{\min(m+2,3)}$ for $H_\varepsilon^{m,k}$. That is, no matter how many moment conditions that are fulfilled, an analytical error proportional to ε^3 is the best that can be achieved. The approximations $H_\varepsilon^{2,1}$, $H_\varepsilon^{2,2}$ and $H_\varepsilon^{4,1}$ are all effected by this cap. Compare to figure 4 in the previous section, in which case the analytical error is proportional to ε^{m+2}.

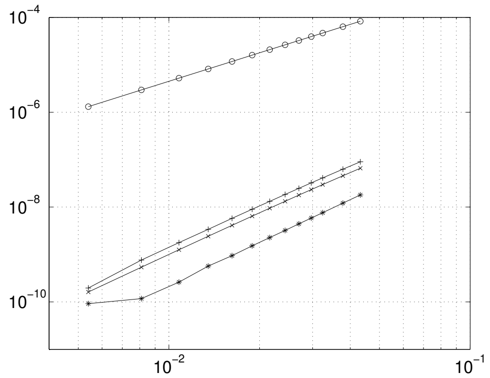

Figure 5: Plot of end point error (error at $x = 1$) versus ε for different approximations of the Heaviside function: $H_\varepsilon^{0,0}$ (-$\circ$-), $H_\varepsilon^{2,1}$ (-+-), $H_\varepsilon^{2,2}$ (-$\times$-), $H_\varepsilon^{4,1}$ (-$*$-). The slopes correspond to ε^p, where p is approximately 2, 3, 3 and 3, respectively.

It is possible to derive conditions for higher order accuracy than $O(\varepsilon^3)$ also in the discontinuous coefficient case. From the difference between (23) and the corresponding regularized problem we get

$$\frac{d}{dx}(u - u_\varepsilon) = a(x)\, u - a_\varepsilon(x) u_\varepsilon. \tag{36}$$

With the definition of the error $e(x) = u(x) - u_\varepsilon(x)$ we have

$$\frac{de}{dx} = a_\varepsilon(x)e + u\,(a(x) - a_\varepsilon(x)) \tag{37}$$

$$e(x) = \int_{-\varepsilon}^{x} (a_\varepsilon(\xi)e(\xi) + u(\xi)(a(\xi) - a_\varepsilon(\xi))\,)\,d\xi. \tag{38}$$

The second term in the integral can be controlled by the regular moment conditions for $a - a_\varepsilon$ applied to intervals $(-\varepsilon, 0)$ and $(0, \varepsilon)$, respectively. The general form of the solution $u(\xi)$ is not regular at $\xi = 0$ and we need two separate Taylor expansions. This is however not enough to break the $O(\varepsilon^3)$ barrier. The first term in (38) must also be controlled

$$\int_{-\varepsilon}^{x} (a_\varepsilon(\xi)e(\xi)d\xi = O(\varepsilon^{m+2}). \tag{39}$$

This condition contains the product between the rapidly changing a_ε and u_ε ($e = u - u_\varepsilon$) in the regularization zone. Such interaction does also exist in the cell problem for homogenization of differential equations with rapidly oscillating coefficients [3].

Expressing u in the integral form is also useful for other problems. If

$$\frac{d}{dx}\,(a(x)\frac{\partial u}{\partial x}) = f(x), \qquad -1 \le x \le 1, \tag{40}$$

$$\frac{d}{dx}(a_\varepsilon(x)\frac{\partial u_\varepsilon}{\partial x}) = f(x), \qquad -1 \le x \le 1, \tag{41}$$

$u(-1) = u(1) = u_\varepsilon(-1) = u_\varepsilon(1) = 0$, we have after integration, division by $a(x)$ and $a_\varepsilon(x)$ and integration again

$$\begin{aligned} u(x) - u_\varepsilon(x) = &- \int_{-\varepsilon}^{x} (a(\xi)^{-1} - a_\varepsilon(\xi)^{-1}) \int_{-\varepsilon}^{\xi} f(\eta)d\eta\, d\xi \\ &+ C \int_{-\varepsilon}^{x} (a(\xi)^{-1} - a_\varepsilon(\xi)^{-1})\, d\xi, \end{aligned} \tag{42}$$

where C is determined by $u(1) = u_\varepsilon(1) = 0$.

From (42) we see that moment conditions should apply to the inverses $a^{-1} - a_\varepsilon^{-1}$ and not to $a - a_\varepsilon$. This is also similar to homogenization where the harmonic average produces the correct effective coefficient.

To illustrate the importance of this fact, we study the results from some numerical simulations. Consider the equation (40) with $f(x) = -e^x$ and

$$a(x) = \begin{cases} a_1 = 1, & -1 \le x < x^* \\ a_2 = 2, & x^* < x \le 1, \end{cases} \tag{43}$$

subject to Dirichlet boundary conditions, $u(-1) = 0$, $u(1) = (e^{x^*} + e^1 - 2e^{-1})/2$. This equation has the solution

$$u(x) = \begin{cases} u_1(x) = \frac{1}{2}(e^x - e^{-1}), & -1 \le x \le x^* \\ u_2(x) = u_1(x^*) + \frac{1}{2}(e^x - e^{x*}), & x^* < x \le 1 \end{cases} \tag{44}$$

We use a second order finite difference approximation. We use a small step size $h = 2/N$, with $N = 6400$, to focus on the analytical errors. To measure the error, we use the 2-norm of the difference between the computed solution and the analytical solution for $|x - x^*| > \varepsilon$.

The left plot in the figure 6 shows the results when we apply the regularization to $a(x)^{-1}$, i.e. when we define

$$a_\varepsilon(x) = \frac{1}{a_1^{-1} + H_\varepsilon^{m,k}(x - x^*)(a_2^{-1} - a_1^{-1})}. \tag{45}$$

The results are shown for $H_\varepsilon^{0,0}$ (i.e the piecewise linear approximation), and $H_\varepsilon^{2,1}$ as defined in (17)-(18). The slopes in the figure corresponds to errors proportional to ε^p, with p close to 2 and 4, respectively. This is what was predicted from the moment conditions. In the right plot of the same figure, we plot the results when we use the same Heaviside approximations, but instead use them to regularize $a(x)$ directly, i.e. define

$$a_\varepsilon(x) = a_1 + H_\varepsilon^{m,k}(x - x^*)(a_2 - a_1). \tag{46}$$

Here, the analytical errors are much larger. No moment conditions are fulfilled, and we see a behaviour of ε^p, where p is close to 1 for both approximations.

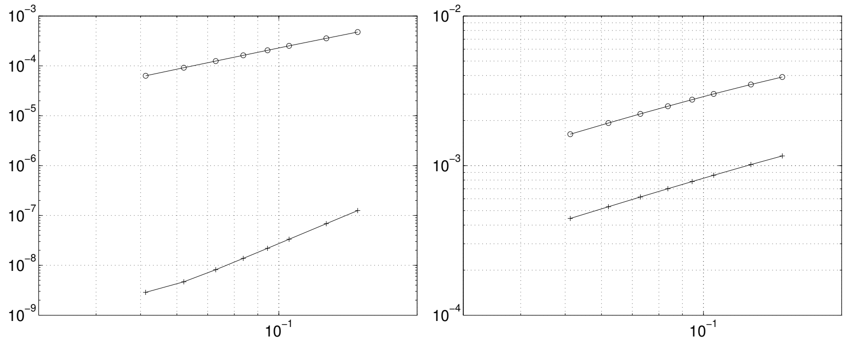

Figure 6: Plot of error versus ε for two different approximations of the Heaviside function: $H_\varepsilon^{0,0}$ (-o-) and $H_\varepsilon^{2,1}$ (-+-). In the left figure, the regularization is applied to $1/a(x)$ (45), and in the right it is applied to $a(x)$ (46). Note the different scales on the y-axes.

Now, consider the equation,

$$-\frac{\partial}{\partial x}(a(x,y)\frac{\partial u}{\partial x}) - \frac{\partial}{\partial y}(a(x,y)\frac{\partial u}{\partial y}) + u = f(x) \quad -1 \leq x, y \leq 1, \tag{47}$$

where $f(x) = 8\sin(\pi x) + 5\cos(2\pi x) + 4\sin(\pi y)$, with periodic boundary conditions. We let $a(x,y)$ be piecewise constant, with one value inside the circle of radius r centered in (x_c, y_c), and another value outside, i.e.

$$a(x,y) = \begin{cases} a_1 = 1, & ((x - x_c)^2 + (y - yc)^2)^{1/2} > r \\ a_2 = 10, & ((x - x_c)^2 + (y - yc)^2)^{1/2} \leq r \end{cases} \tag{48}$$

We solve this equation by a standard second order finite difference method. In analogy to (45), we regularize $a(x,y)^{-1}$, using $H_\varepsilon^{2,2}$ as defined in (17)-(18). We use a regular grid with step size $h = 2/N$ in both directions. The numerical solutions are plotted for $N = 80, 160$ and 320 in figure 7. The width of the transition zone $\varepsilon = 4\,h$.

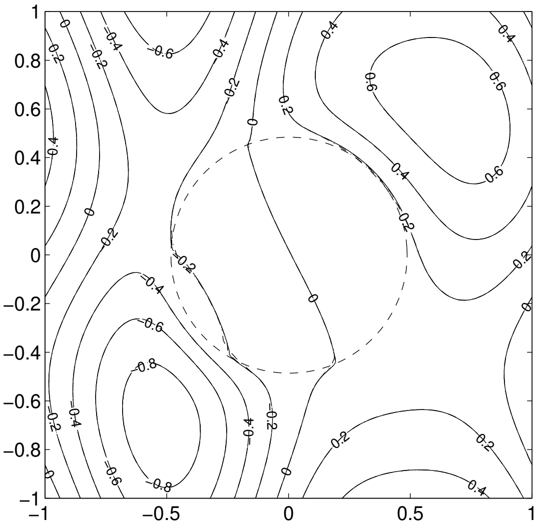

Figure 7: The numerical solution of (47) is plotted for $N = 80$, 160, 320. The dashed line indicates the circle at which $a(x,y)$ is discontinuous ($r = 0.485$, $(x_c, y_c) = \frac{1}{160}(\frac{1}{3}, -\frac{1}{6})$).

For this problem we have no exact solution to compare with to compute the error. Instead we compare the consecutive solutions on grid sizes 80×80, 160×160 and 320×320 points. We do this both for the numerical approximation based on $H_\varepsilon^{2,2}$, and for the case when $a(x,y)$ is kept discontinuous. In the first case, there will be both analytical and numerical errors present, whereas in the second case there will be no analytical error. From the results in table 1 we can see that the total error in the case where $1/a$ is regularized is smaller than in the case where it is not, and that the convergence rate is better. The error is measured in 1-norm, i.e. as the average of the absolute value, outside of the transition zone.

Approximation of $1/a$	$\|\|v_{h_0} - v_{h_0/2}\|\|_1$	$\|\|v_{h_0/2} - v_{h_0/4}\|\|_1$	p
Discontinuous	$7.39 \cdot 10^{-4}$	$3.23 \cdot 10^{-4}$	1.19
Based on $H_\varepsilon^{2,2}$ $(\varepsilon = 4h)$	$2.83 \cdot 10^{-4}$	$6.83 \cdot 10^{-5}$	2.05

Table 1: The errors and measured order of convergence p in the numerical solution of (47). The step size $h = h_0$, $h_0/2$ and $h_0/4$ with h_0=$2/80 = 0.025$.

5 Boundary Conditions and Other Applications of Regularization

The regularization technique can also be used in the numerical approximation of boundary conditions. A natural application is when the boundary is irregularly located in a regular computational grid.

The first step is to introduce the boundary condition as δ-function sources in the differential equation. Compare the, so called, Heugens surface conditions in computational electromagnetics, [13]. In the second step the δ-function sources are regularized followed by a discretization of the regularized problem.

Let us first consider a simple hyperbolic system

$$\begin{aligned} \frac{\partial u}{\partial t} + \frac{\partial u}{\partial x} &= f_1 \\ \frac{\partial v}{\partial t} + \frac{\partial v}{\partial y} &= f_2 \end{aligned} \tag{49}$$

where $x \in \Omega$, $t > 0$. The boundary conditions are given by

$$\begin{cases} u = g_1, & x \in \partial\Omega_1 \\ v = au + g_2 & x \in \partial\Omega_2, \end{cases}$$

and the domain is defined as

$$\begin{aligned} \Omega &= \{(x,y),\ \alpha x + \beta < y < 1,\ -1 < x < 1\} \\ \partial\Omega_1 &= \{(x,y),\ x = 0,\ \beta < y \leq 1 \\ \partial\Omega_2 &= \{(x,y),\ y = \alpha x + \beta,\ 0 \leq x \leq 1\}. \end{aligned}$$

Our source term formulation is

$$\begin{aligned} \frac{\partial u}{\partial t} + \frac{\partial u}{\partial x} &= f_1 \\ \frac{\partial v}{\partial t} + \frac{\partial v}{\partial y} &= H(y - \alpha x - \beta) f_2 + \delta(y - \alpha x - \beta)(au + g_2) \end{aligned} \tag{51}$$

in the domain $\tilde{\Omega} = \{(x,y),\ -1 < x < 1,\ -1 < y < 1\}$ and the boundary conditions are

$$\begin{aligned} u &= g, & x &\in \partial\Omega_1 \\ v &= 0, & y &= 0,\ -1 \leq x \leq 1. \end{aligned}$$

Note that the Heaviside function is used to eliminate build up of values in v outside of Ω.

For a numerical test we choose

$$a = 1, f_1 = 0,\ f_2 = 1,\ g = \sin(\pi t),\ g_2 = 0,\ \alpha = 0.5,\ \beta = 0.3$$

which gives the solution

$$v = -\sin(\pi(t - y - \alpha x - \beta)) + y - \alpha x + \beta. \tag{52}$$

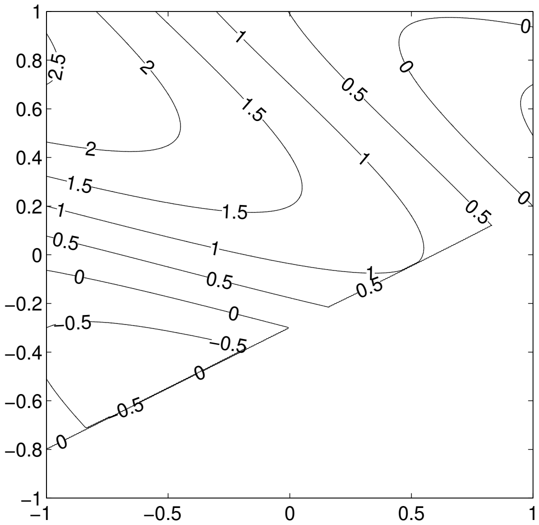

Figure 8: The analytic solution v at $t = 4.0$, as given by (52).

The solution is plotted in figure 8.

The discretization is made using a Lax-Wendroff scheme, which is second order accurate. We solve both the original problem (49) and the reformulated problem (51) using a regular grid on $([-1,1] \times [-1,1])$, with grid size $h = 2/N$ in both directions. For the original problem, the boundary conditions for v is set on the stair cased boundary in the grid, approximating $\partial\Omega_2$, i.e. the line $y = 0.5x + 0.3$. For the reformulated problem (51), the Heaviside function and the δ-function are replaced by piecewise linear approximations, with $\varepsilon = 2h$.

The error compared to the analytical solution is measured above the transition region, i.e for $y \geq -0.3 + 0.5x + \varepsilon$. We use the 1-norm, i.e. the average of the absolute value of the error in this region. The results are displayed in table 2. In the original problem, the stair casing effect reduces the order of convergence to first order. The errors are also much larger than the errors obtained when solving the reformulated problem (51), where the second order accuracy of the Lax-Wendroff method is retained.

N	$\|v_N - v\|_1$	p
50	$1.14 \cdot 10^{-2}$	–
100	$5.99 \cdot 10^{-3}$	0.92
200	$3.08 \cdot 10^{-3}$	0.96
400	$1.56 \cdot 10^{-3}$	0.98

N	$\|v_N - v\|_1$	p
50	$4.99 \cdot 10^{-4}$	–
100	$1.12 \cdot 10^{-4}$	2.16
200	$2.66 \cdot 10^{-5}$	2.07
400	$6.51 \cdot 10^{-6}$	2.03

Table 2: Errors and measured order of convergence p for numerical solution at $t = 4.0$ of (49) (left table) and (51) (right table).

This technique generalizes to wider classes of problems. Consider, for example, a general hyperbolic system in the domain $(x,y) \in \Omega \subset \mathbb{R}^2$,

$$\frac{\partial}{\partial t}\begin{pmatrix} u_1 \\ u_2 \end{pmatrix} + \begin{pmatrix} A_{11} & 0 \\ 0 & A_{22} \end{pmatrix} \frac{\partial}{\partial x}\begin{pmatrix} u_1 \\ u_2 \end{pmatrix} + \begin{pmatrix} B_{11} & B_{12} \\ B_{21} & B_{22} \end{pmatrix} \frac{\partial}{\partial y}\begin{pmatrix} u_1 \\ u_2 \end{pmatrix} = \begin{pmatrix} f_1 \\ f_2 \end{pmatrix} \quad (53)$$

for which the eigenvalues of A_{11} and A_{22} are positive and negative respectively.

We have here chosen the boundary point $(x,y) \in \partial\Omega$, $x = x^*$ such that the inward normal to the boundary $\partial\Omega$ is in the positive x-direction. The localization to $x = x^*$ and the decomposition of the matrix in front of the x-derivative in the hyperbolic system is done in order to formulate well posed boundary conditions [7],

$$u_1 = Ru_2 + g_1 \quad (x,y) \in \partial\Omega,\ x = x^*.$$

The natural generalization of (51) for the incoming components u_1, is

$$\frac{\partial u_1}{\partial t} + A_{11}\frac{\partial u_1}{\partial x} + B_{22}\frac{\partial u_1}{\partial y} = H(x)\left(f_1 - B_{12}\frac{\partial u_2}{\partial y}\right) + \delta(x) A_{11}^{-1}(Ru_2 - g).$$

We shall briefly discuss two applications in computational physics for which regularization has recently been used: one in multiphase flow and one in computational electromagnetics.

In the first application incompressible, immiscible multiphase flow in two dimensions was considered. The equations describing this flow are the Navier-Stokes equations for incompressible flow, (56)-(57). We assume that we have two different fluids, fluid A and fluid B separated by the interface Γ. The density and viscosity at a fixed time are given by

$$(\rho(x), \mu(x)) = \begin{cases} (\rho_A, \mu_A) & \text{for } x \text{ in fluid } A, \\ (\rho_B, \mu_B) & \text{for } x \text{ in fluid } B. \end{cases}$$

In general $\rho_A \neq \rho_B$ and $\mu_A \neq \mu_B$, so that the density and viscosity are discontinuous at the interface $\Gamma = \Gamma(t)$. The Navier-Stokes equations can be written as

$$\rho\left(\frac{\partial u}{\partial t} + u \cdot \nabla u\right) = -\nabla p + \nabla \cdot (\mu(\nabla u + \nabla u^T))f + \rho g, \quad (56)$$

$$\nabla \cdot u = 0, \quad (57)$$

in $\Omega \subset \mathbb{R}^2$, together with boundary conditions $u = \nu$ on $\partial\Omega$. In addition, we need to specify an appropriate initial condition for the velocity field $u(x,t)$. In the above equations $p(x,t)$ denotes the pressure field. Buoyancy effects arises from the source term ρg, where g is the gravitational force. The surface tension force f is given by

$$f = \sigma \kappa \hat{n} \delta_\Gamma \quad (58)$$

where δ_Γ is a measure of delta function type with support on Γ. Further, $\sigma \in \mathbb{R}$ is the surface tension coefficient, $\kappa \in \mathbb{R}$ is the curvature and $\hat{n} \in \mathbb{R}^2$ is a normal vector to the interface Γ. At every point along an interface Γ, the direction of this force is towards the local center of curvature. The interface Γ is advected by the velocity field u.

A formally second order finite element method was used and the discontinuous coefficients $\rho(x,t)$ and $\mu(x,t)$ was regularized, see [16]. The singular source term f was handled as a line integral in the weak formulation. The computations show that the regularization generated a convergence rate of second order. The approximative functions $\rho_\varepsilon \in C^1$ and $\mu_\varepsilon \in C^1$ had two matching moments. For details see [14].

For the electromagnetics application consider time domain simulations of the Maxwell's equations in a three dimensional spatial domain with a wire,

$$\mu \frac{\partial H}{\partial t} = -\nabla x E \tag{59}$$

$$\varepsilon \frac{\partial E}{\partial t} = \nabla x H - \sigma E - I/A \tag{60}$$

$$C \frac{\partial V}{\partial t} + \frac{\partial I}{\partial \xi} = 0 \tag{61}$$

$$L \frac{\partial I}{\partial t} + \frac{\partial V}{\partial \xi} = E - RI \tag{62}$$

where $H(x,t), E(x,t), \mathbb{R}^{3+1} \to \mathbb{R}^3$ are the magnetic and electric fields respectively. The voltage V and the current I in the wire are given as function of time and arc length ξ. The other terms describe material properties.

Regularization was used for the delta function source term I/A in (60). This term can be written $I(\xi(x),t)\delta_\Gamma(x)$ where Γ indicates the location of the wire which is not aligned with the Cartesian grid. The function δ_Γ was regularized by a C^0 approximation with two matching moments. The computational results show a dramatic improvement over the standard technique of numerically aligning the wire with the grid, see [8]. The Yee-scheme was used for the discretization of the Maxwell's equations, see [13].

6 Direct Discretization

In this paper we have divided the numerical regularization process into two steps. In the first the singular functions are regularized, and in the second, the regularized differential equation is discretized. This simplifies the analysis and is also advantageous since the regularized problem can be approximated by a variety of standard numerical methods.

It may sometimes be desirable to have a very small transition zone and then it is natural to consider a direct discretization of a singularity. We shall here make a few useful observations in the case of source terms and come back with a more detailed study in a forthcoming paper.

Let us first consider a δ-function source in one dimension, and show that it is possible to have a perfect approximation for some problems. We start by approximating the simple equation

$$\frac{\partial u}{\partial x} = \delta(x - x^*), \qquad u(0) = 0,\ x^* > 0$$

by a standard numerical method, as for example the Euler scheme or the trapezoidal rule. Furthermore, we introduce $\delta_\varepsilon(\xi)$ as an approximation to the delta function with support on $-\varepsilon < \xi < \varepsilon$. The approximation of the solution to the equation above for $x > x^* + \varepsilon$ is then given by the sum

$$\Sigma(\delta_\varepsilon) = h \sum_{i=0}^{n-1} \delta_\varepsilon(x_i - x^*), \tag{64}$$

where the x_i's are grid points ($x_i = h\,i$, $i = 0, \ldots, N$), with $x_{n-1} \leq x^* + \varepsilon < x_n$.

One simple approximation of the delta function is the hat function

$$\delta_L(\xi) = \begin{cases} \frac{1}{\varepsilon^2}(\xi + \varepsilon) & \text{if } -\varepsilon \leq \xi < 0, \\ \frac{1}{\varepsilon^2}(\varepsilon - \xi) & \text{if } 0 \leq \xi \leq \varepsilon, \\ 0 & \text{if } |\xi| > \varepsilon, \end{cases} \tag{65}$$

Write $x^* = x_k + q\Delta x$, with x_k being the x-value of the closest grid point to the left of x^*. With $\varepsilon = p\Delta x$, the sum (64) evaluates as

$$\Sigma(\delta_L) = \frac{1}{p^2}((k_0 + k_1 + 1)p + (k_1 - k_0 - 1)q - \frac{k_0(k_0+1)}{2} - \frac{k_1(k_1+1)}{2}) \tag{66}$$

where

$$\begin{aligned} k_0 &= \lfloor p - q \rfloor \\ k_1 &= \lfloor p + q \rfloor \end{aligned} \tag{67}$$

This formula yields that we get an exact result outside of the transition zone ($|x - x^*| > \varepsilon$) if p is an integer. The result is then exact independently of the choice of q, that is, independently of how the grid is shifted relative to the location of δ_L.

Another simple, and commonly used approximation of the delta function is the cosine approximation ([10, 12])

$$\delta_C(\xi) = \begin{cases} (1 + \cos(\pi\xi/\varepsilon))/2\varepsilon & \text{if } |\xi| < \varepsilon, \\ 0 & \text{if } |\xi| \geq \varepsilon, \end{cases} \tag{68}$$

For this approximation the sum (64) evaluates as

$$\Sigma(\delta_C) = \frac{k_0 + k_1 + 1}{2p} + \frac{\sin((k_0 + k_1 + 1)\pi/2p)\ \cos(((k_1 - k_0)/2 - q)\pi/p)}{2p\ \sin(\pi/2p)}, \tag{69}$$

with k_0 and k_1 as before (67). This formula evaluates exactly to 1 as long as $2p$ is an integer.

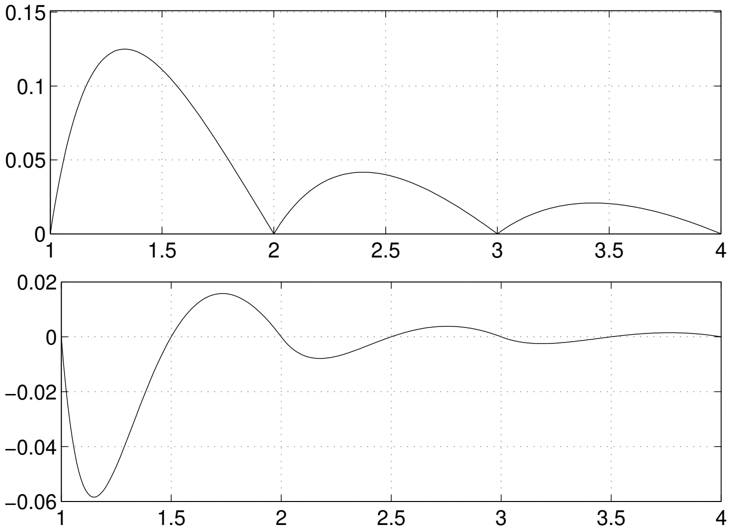

Figure 9: $\Sigma - 1.0$ plotted versus p for $q = 0.0$. Top figure: linear approximation ($\Sigma(\delta_L) - 1.0$), bottom figure: cosine approximation ($\Sigma(\delta_C) - 1.0$).

If p is not an integer for the linear approximation, or $2p$ is different from an integer in the cosine approximation, then there is an $O(1)$ error in the approximation which is given in figure 9. The exact integration property is lost if p is changed, that is, under dilation.

In one dimension, p equals an integer is an efficient choice but in more than one dimension and with the multi-dimensional extension

$$\delta_\Gamma(\mathbf{x}) \sim \delta_\varepsilon(\mathrm{dist}(\mathbf{x}, \Gamma)) \tag{70}$$

different angles between a line Γ and the axes of the computational grid will in effect correspond to variations in p. The excellent result from one dimension does not extend to the multidimensional case. As an example we study the equation

$$\frac{\partial u}{\partial x} + a\frac{\partial u}{\partial y} = f(x,y) \tag{71}$$

with $f(x,y) = \delta(d(x,y))$. Here, d is the signed distance to the line Γ, described by $y = \alpha(x - x_0)$. We denote the angle between Γ and the x-axis by $\theta = \tan(\alpha)$.

The solution of this problem is given by

$$u(x,y) = \begin{cases} 0 & \text{if } d(x,y) < 0, \\ 0 & \text{if } d(x,y) > 0, \text{ but the characteristic} \\ & \text{through (x,y) never intersected } \Gamma. \\ A & \text{if } d(x,y) > 0, \textit{ and} \text{ the characteristica} \\ & \text{through (x,y) has intersected } \Gamma. \end{cases} \tag{72}$$

with

$$A = \frac{1}{|\sin\theta - a\ \cos\theta|}. \tag{73}$$

We discretize (71) simply by:

$$D_x^+ u_{i,j} + aD_y^- u_{i,j} = f(x_i, y_j). \tag{74}$$

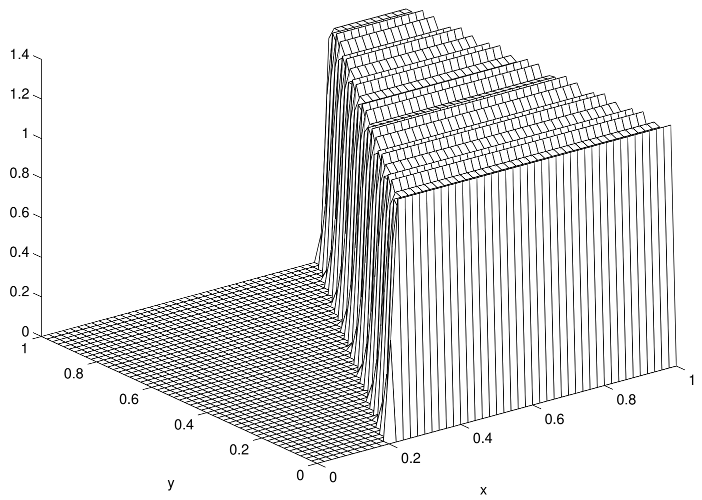

Figure 10: Solution of (71) with $a = 0$, using $\delta_C(d(x, y))$. The line Γ, makes a $60°$ angle with the x-axis ($\theta = 60°$). The solution is plotted for $p = 1$ in which case the maximum relative error in the solution at $x = 1.0$ is slightly above 4.5%. For $p = 2$, the same error is about 0.6%.

In figure 10 we see that the exact integration property is lost in two dimensions. This result was obtained for the cosine approximation. The errors for the linear approximation would be even larger.

In our final observation we shall see that it is possible to derive an approximative δ-function with the perfect integration property ($\Sigma(\delta_\varepsilon) = 1$) for all shifts and a range of dilations.

We define the function $\varphi(x)$ from its Fourier transform $\hat{\varphi}(\omega)$. We have that

$$\hat{\varphi}(0) = \int_{-\infty}^{\infty} \varphi(x)dx. \tag{75}$$

The Poisson's summation formula reads

$$\sum_j \hat{\varphi}(j) = \sum_j \varphi(j) \tag{76}$$

If the function $\hat{\varphi}(\omega)$ has a compact support on $\omega \in [-\beta, \beta]$, $\beta < 1 - \sigma$, $\sigma > 0$, then this yields

$$\hat{\varphi}(0) = \sum_j \varphi(j). \tag{77}$$

The Poisson's summation formula can be scaled as

$$\sum_j \hat{\varphi}(j/\alpha) = \alpha \sum_j \varphi(\alpha j). \tag{78}$$

So, we have that for $\alpha \leq 1$,

$$\alpha \sum_j \varphi(\alpha j) = \sum_j \hat{\varphi}(j/\alpha) = \hat{\varphi}(0) = \int_{-\infty}^{\infty} \varphi(x) dx. \tag{79}$$

We will use this formula to design a delta function approximation which has the perfect integration property.

We have chosen to define $\hat{\varphi}(\omega)$ by

$$\hat{\varphi}(\omega) = \begin{cases} e^{\frac{1}{d\beta^2}} e^{\frac{1}{d(\omega^2 - \beta^2)}} & |\omega| < \beta, \\ 0 & |\omega| \geq \beta, \end{cases} \tag{80}$$

with $d = 0.1$ and $\beta = 1.0$. A plot of $\hat{\varphi}(\omega)$ is shown in figure 11.

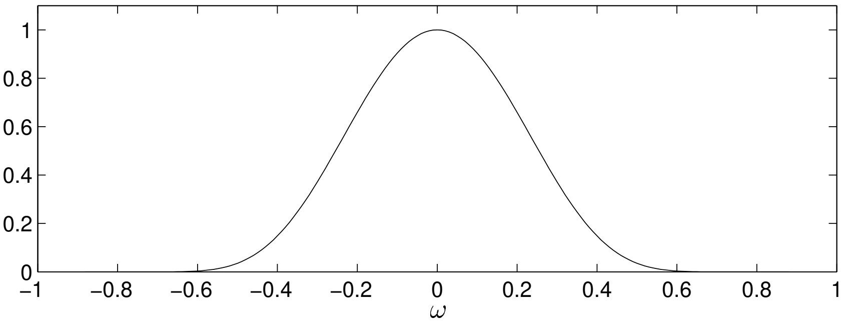

Figure 11: The Fourier spectrum $\hat{\varphi}(\omega)$ plotted versus ω.

We evaluate $\varphi(z)$ from this Fourier spectrum through

$$\varphi(z) = \int_{-\infty}^{\infty} \hat{\varphi}(\omega) e^{2\pi i \omega z} dz = \int_{-1}^{1} \hat{\varphi}(\omega) e^{2\pi i \omega z} dz \tag{81}$$

In Figure 12, $\varphi(z)$ corresponding to the given $\hat{\varphi}(\omega)$, is plotted. To define a δ-function approximation on the computational grid, $\varphi(z)$ will be scaled with h, i.e. we define

$$\delta_F(\xi) = (\gamma h)^{-1} \varphi(\xi/(\gamma h)), \tag{82}$$

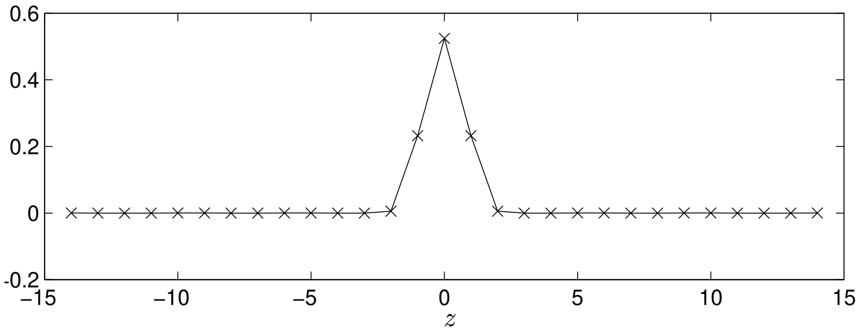

Figure 12: $\varphi(z)$ corresponding to $\hat{\varphi}(\omega)$ given by (80).

where the constant $\gamma \approx 1$. Due to the summation property (79), this delta function approximation will have the perfect integration property. It does however not have compact support. As seen in figure 12 the exponential decay is rapid and $\varphi(z)$ can be truncated to a compact support in a practical simulation.

The crucial question is of course how this function will behave when used in the two dimensional problem that was discussed in the previous section. In that case, the effective width of the spike in the x-direction is altered, and the spike is shifted differently compared to the grid in the x-direction for different y values. A test of this case for a few different values of θ show very small errors compared to the analytical solution, and no dependence on the shift q can be found.

If we define the signed distance function $d(x, y)$ as before, then we can use $\delta_F(d(x, y))$ as an approximation of the delta function. In Figure 13, the solution found for $a = 0$ and $\theta = 60°$ is plotted. This should be compared to the solution plotted in Figure 10. The absence of oscillations in the solution confirms that the error does not depend on the shift q. The error is also much smaller in magnitude.

It should be noted that we considered a problem that did not require higher moment conditions in this section. In section 3 we saw that such conditions may in principle be introduced by having

$$\left.\frac{d^k \hat{\varphi}(\omega)}{d\omega^k}\right|_{\omega=0} = 0 \qquad \text{for } k = 1, 2, \ldots, K. \tag{83}$$

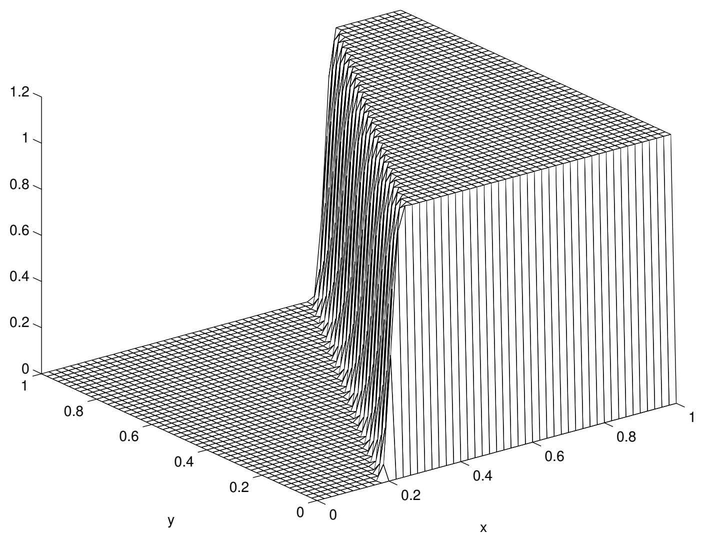

Figure 13: Solution of (71) with $a = 0$, using $\delta_F(d(x, y))$. The line Γ, describing the position of the delta function, makes a 60° angle with the x-axis ($\theta = 60^\circ$). The maximum relative error in the solution at $x = 1.0$ is less than 10^{-9}.

References

[1] S. Abarbanel, D. Gottlieb and E. Tadmor, *Spectral methods for discontinuous problems*, Proceedings of the 1985 Conference on Numerical Method for Fluid Dynamics II, Clarendon Press, Oxford, 101-135, 1986.

[2] J.T. Beale and A. Majda, *Vortex methods. II: Higher order accuracy in two and three dimensions*, Mathematics of Computation, 39:29-52, 1982.

[3] A. Bensoussan, J.-L. Lions and G. Papanicolaou, *Asymptotic analysis for periodic structures*, North Holland, 1978.

[4] G. Beylkin, *On the fast Fourier transform of functions with singularities*, Applied and Computational Harmonic Analysis, 2:363-381, 1995.

[5] A. Ditkowski, K. Dridi, J.S. Hesthaven, *Convergent Cartesian grid methods for Maxwell's equations in complex geometries*, Journal of Computational Physics, Vol. 170, No. 1, 2001, pp. 39-80.

[6] R. Glowinski, T.W. Pan, T.I. Hesla, and D.D. Joseph, *A distributed Lagrange multiplier/fictitious domain method for particulate flows*, International Journal of Multiphase Flow, 25:755-794, 1999.

[7] H.-O. Kreiss and J. Lorenz, *Initial-boundary value problems and the Navier-Stokes equations*, Academic Press, New York, 1989.

[8] G. Ledfelt, *Hybrid time-domain methods and wire models for computational electromagnetics*, TRITA-NA-0106, KTH 2001.

[9] R.J. LeVeque and Z. Li, *The immersed interface method for elliptic equations with discontinuous coefficients and singular sources*, SIAM Journal on Numerical Analysis **31**, 1019-1044, 1994.

[10] C. S. Peskin, *Numerical analysis of blood flow in the heart*, Journal of Computational Physics, 25:220-252, 1977.

[11] C.S. Peskin *The immersed boundary method.* Acta Numerica, 11, 2002. To appear.

[12] M. Sussman, P. Smereka and S. Osher, *A level set approach for computing solutions to incompressible two-phase flow*, Journal of Computational Physics, 114:146-159, 1994.

[13] A. Taflove and S.C. Hagness, *Computational electrodynamics: The finite-difference time domain method*, 2nd ed. Norwood, MA:Artech House, 2000.

[14] A.-K. Tornberg. Interface tracking methods with applications to multiphase flows. Ph.D. Thesis, Department of Numerical Analysis and Computer Science, Royal Institute of Technology (KTH), Stockholm, Sweden, 2000. ISBN 91-7170-558-9, TRITA-NA 0010.

[15] A.-K. Tornberg, *Multi-dimensional quadrature of singular and discontinuous functions*, BIT, to appear.

[16] A.-K. Tornberg and B. Engquist, *A finite element based level set method for multiphase flow applications*, Computing Visualization in Science, 3:93-101, 2000.

[17] S.O. Unverdi and G. Tryggvason, *A front-tracking method for viscous incompressible, multi-fluid flows*, Journal of Computational Physics, 100:25-37, 1992.